Electronic Supplementary Information (ESI)

Optimizing horizontal dipole orientation and dipole-dipole interaction of thermally activated delayed fluorescent emitters for highly efficiency and low roll-off red OLEDs

Jianwen Qin, Xianfeng Qiao, Dezhi Yang, Qian Sun, Yanfeng Dai, Xuhui Zhu, and Dongge Ma*

Institute of Polymer Optoelectronic Materials and Devices, Guangdong-Hong Kong-Macao Joint Laboratory of Optoelectronic and Magnetic Functional Materials, Guangdong Provincial Key Laboratory of Luminescence from Molecular Aggregates, State Key Laboratory of Luminescent Materials and Devices, South China University of Technology, Guangzhou 510640, China

E-mail: msdgma@scut.edu.cn

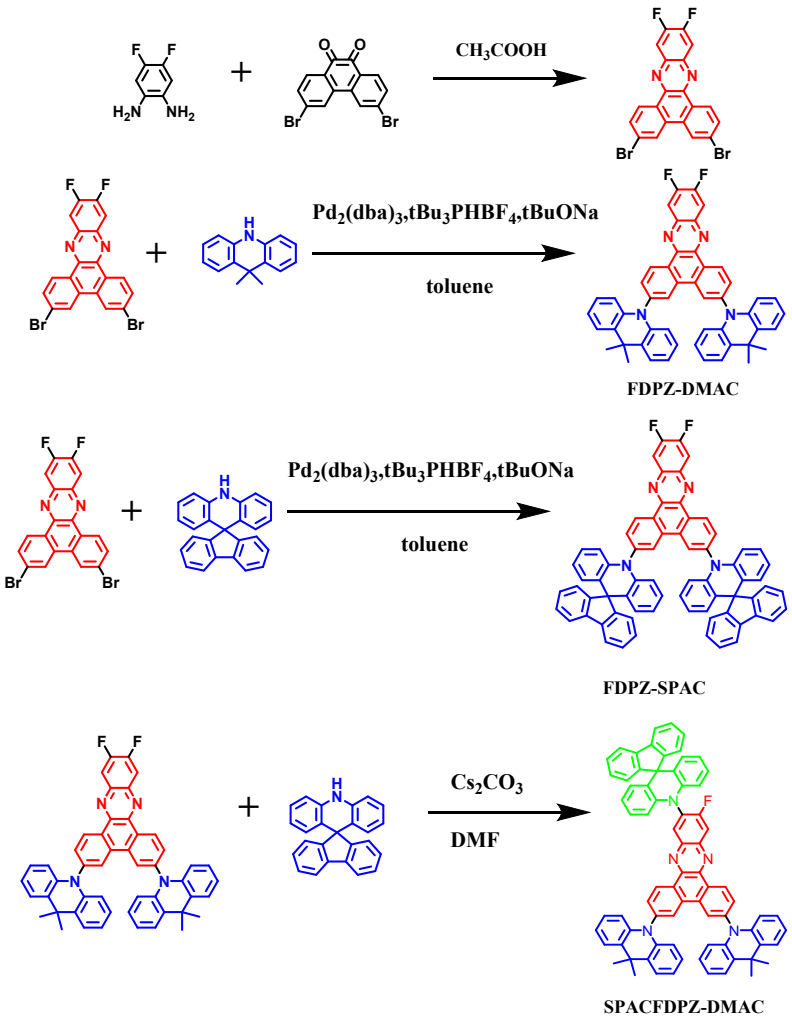

Scheme S1. Synthetic routes of FDPZ-SPAC, FDPZ-DMAC and SPACFDPZ-DMAC three compounds.

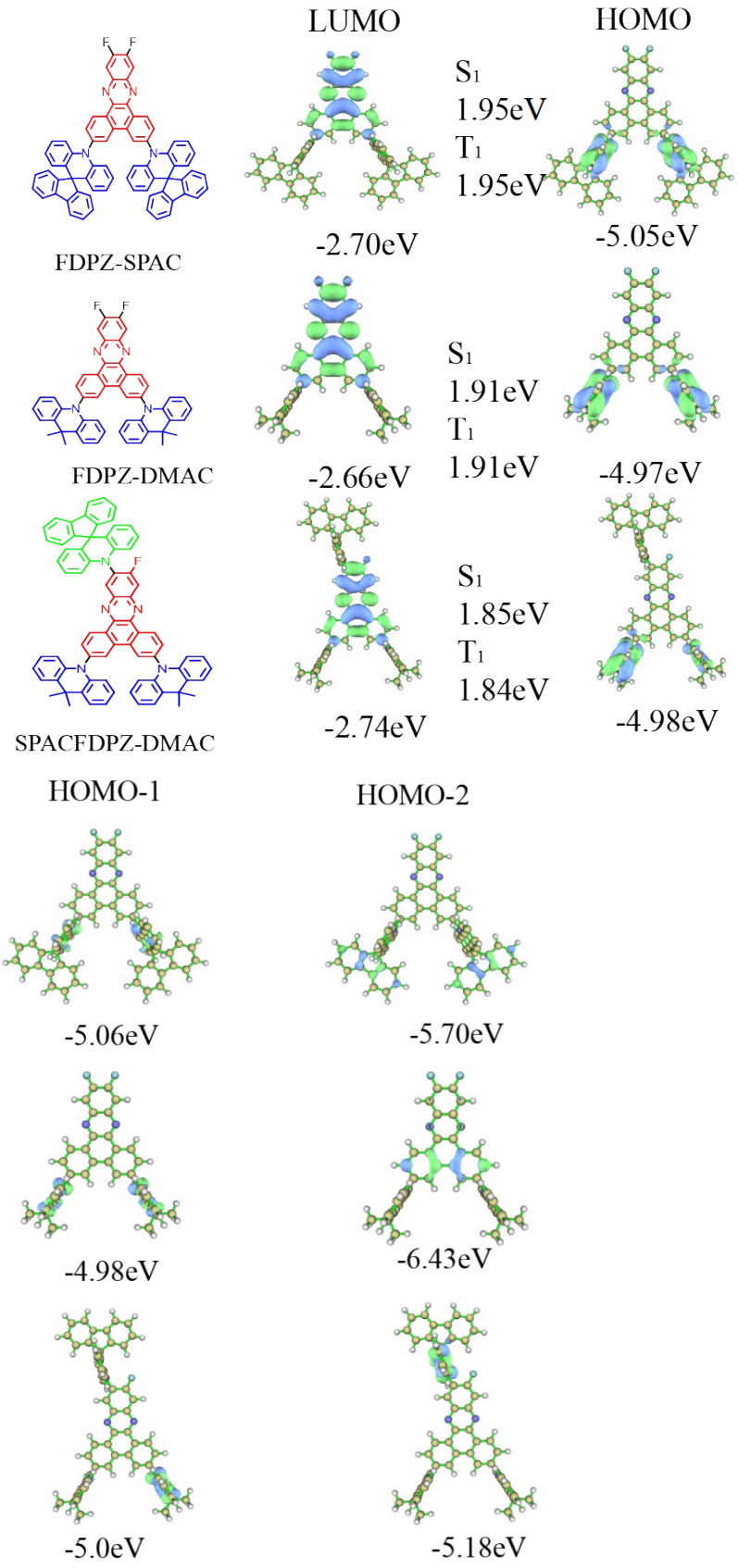

Figure S1. HOMO/LUMO distributions, S_1 and T_1 of FDPZ-SPAC, FDPZ-DMAC and SPACFDPZ-DMAC.

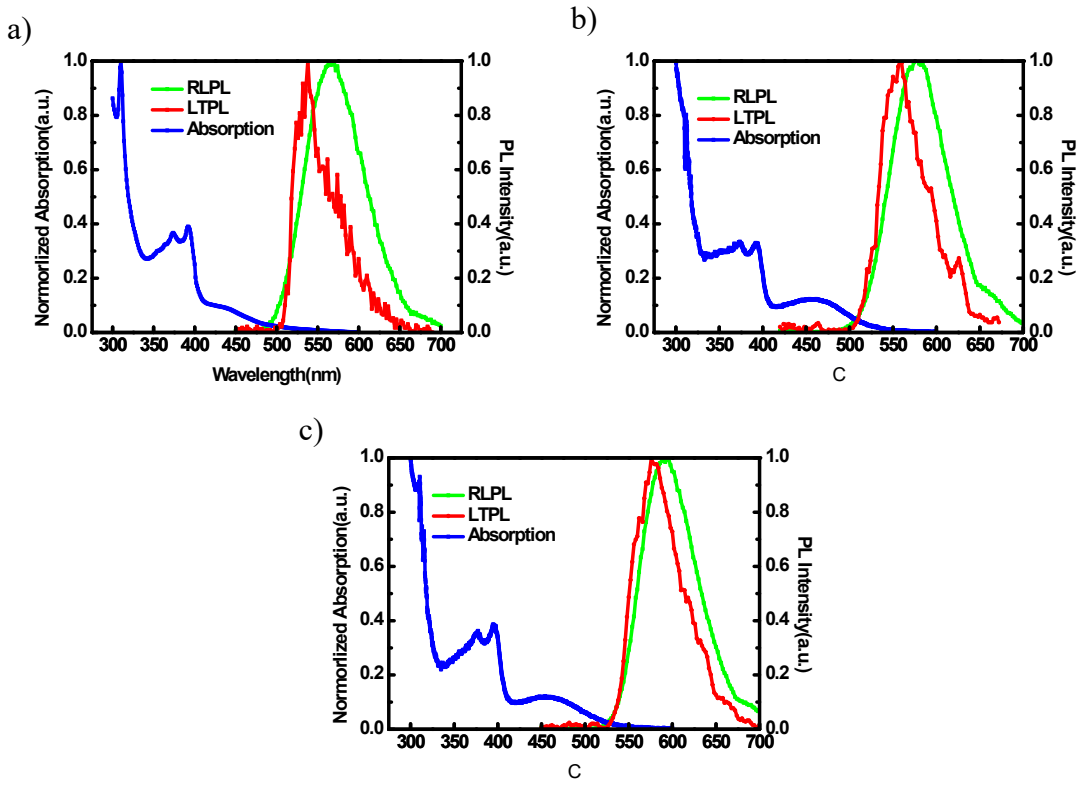

Figure S2. Normalized UV–vis absorption, fluorescence and phosphorescence spectra of a) FDPZ-SPAC, b) FDPZ-DMAC and c) SPACFDPZ-DMAC in toluene.

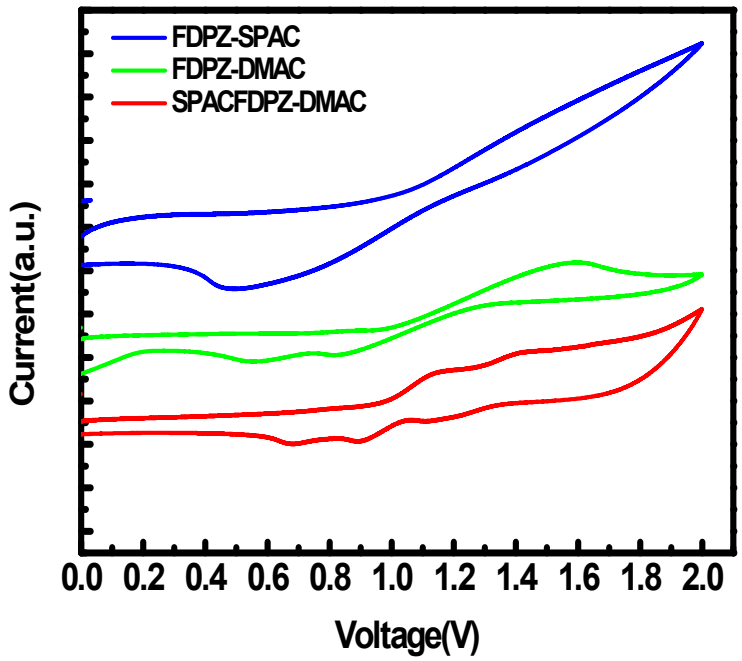

Figure S3. Cyclic voltammetry of FDPZ-SPAC, FDPZ-DMAC and SPACFDPZ-DMAC in CH_3Cl_3

using ferrocene as an internal reference and n-Bu_4NPF_6 (0.1 M) as the supporting electrolyte.

	λabs(nm)	**λ_{PL}(nm)**	**λ_{LTPH}(nm)**	**S_1(eV)**	**T_1(eV)**	**ΔE_{ST}(eV)**	**FWHM(nm)**
FDPZ-SPAC	**434**	**566**	**538**	**2.41**	**2.37**	**0.04**	**82**
FDPZ-DMAC	**454**	**578**	**558**	**2.40**	**2.35**	**0.05**	**80**
SPACFDPZ-DMAC	**457**	**593**	**577**	**2.30**	**2.29**	**0.01**	**75**

Table S1 Photophysical properties of FDPZ-SPAC, FDPZ-DMAC and SPACFDPZ-DMAC in toluene.

	τp(ns)	**τd(μs)**	**$k_S(10^7 s^{-1})$**	**$k_{ISC}(10^7 s^{-1})$**	**$k_{RISC}(10^5 s^{-1})$**	**HOMO(eV)**	**LUMO(eV)**	**PLQY(%)**
FDPZ-SPAC	**28.3**	**7.1**	**1.1**	**1.5**	**2.5**	**-5.32**	**-2.87**	**53**
FDPZ-DMAC	**22**	**7.2**	**1.6**	**1.6**	**2.2**	**-5.31**	**-2.88**	**55**
SPACFDPZ-DMAC	**24.9**	**5.7**	**1.6**	**2.0**	**3.5**	**-5.28**	**-2.96**	**82**

Table S2 Calculated rate constants of mCBP:5% FDPZ-SPAC/ FDPZ-DMAC / SPACFDPZ-DMAC film by measuring exciton lifetime and PLQY values, and HOMO and LUMO values in CH_3Cl_3.

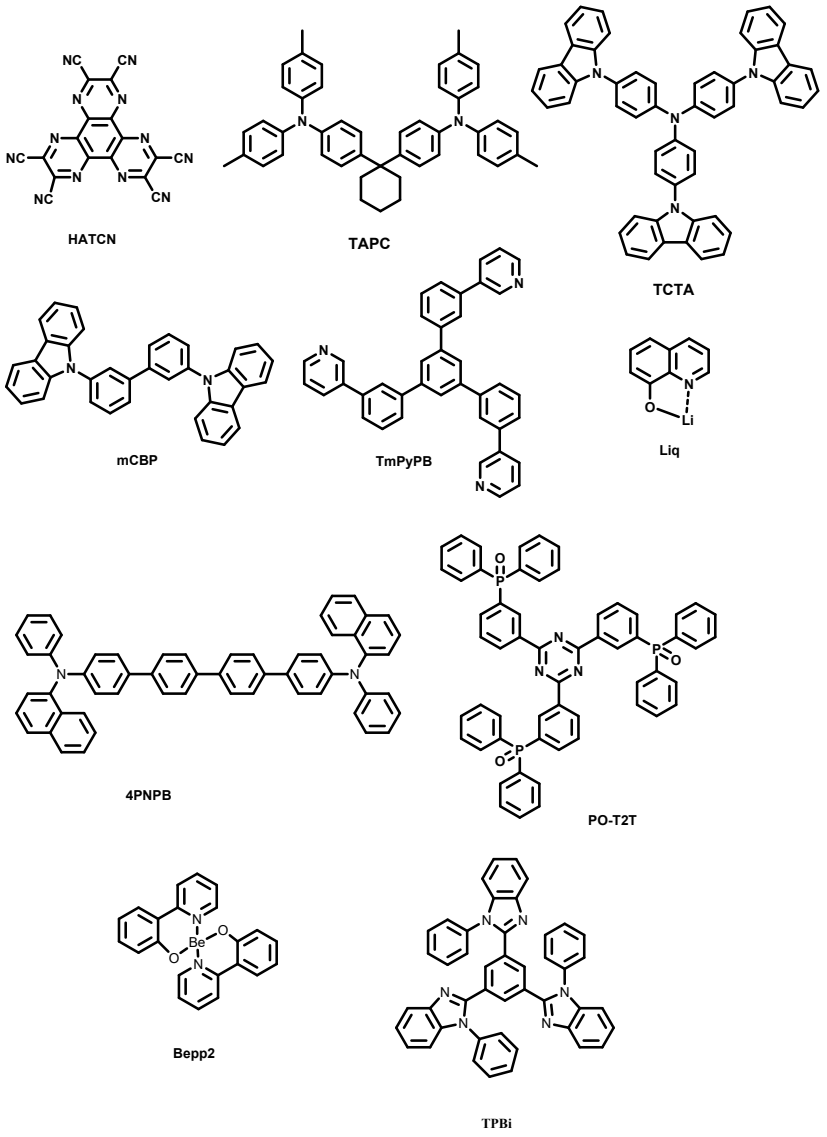

Figure S4. Molecular structures of HATCN, TAPC, TCTA, mCBP, TmPyPB, $Bepp_2$, POT2T, 4PNPB, TPBi and Liq.

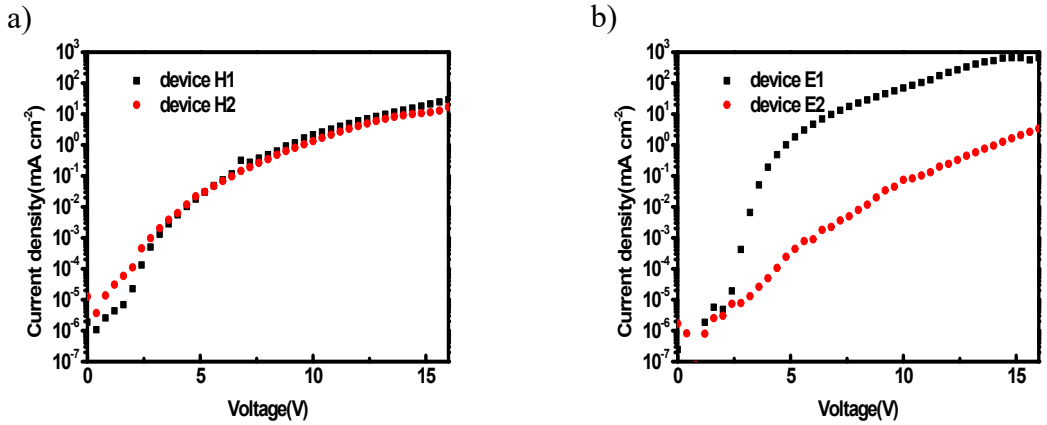

Figure S5. Current density–voltage curves of hole-only device H1 and H2 (hole), and electron-only device E1 and E2 (electron).

Device H1：ITO/HAT-CN (5 nm)/ TAPC (10 nm)/ mCBP (50 nm)/ TAPC (10 nm)/ HAT-CN (5 nm)/ Al (100 nm)

Device H2：ITO/HAT-CN (5 nm)/ TAPC (10 nm)/ mCBP:5%SPACFDPZ-DMAC (50 nm)/ TAPC (10 nm)/ HAT-CN (5 nm)/ Al (100 nm)

Device E1：ITO/Liq (1 nm)/ TmPyPB(10 nm)/ mCBP (50 nm)/ TmPyPB (10 nm)/Liq (1 nm)/ Al (100 nm)

Device E2：ITO/Liq (1 nm)/ TmPyPB(10 nm)/ mCBP:5%SPACFDPZDMAC (50nm)/TmPyPB (10 nm)/Liq (1 nm)/ Al (100 nm)

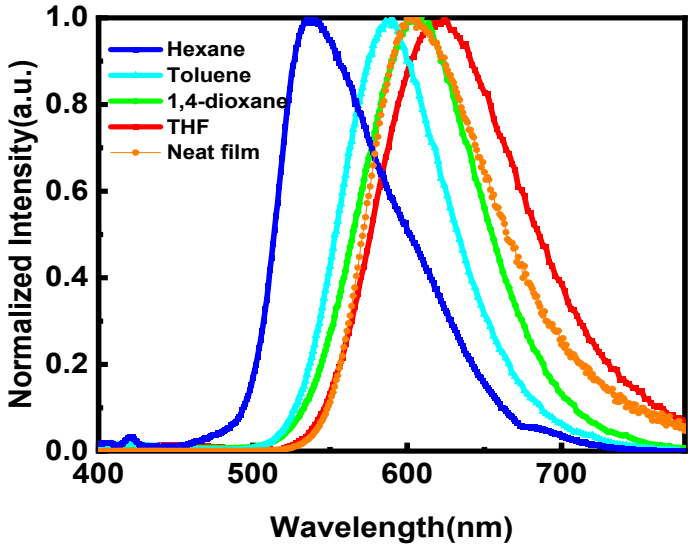

Figure S6. Normalized PL spectra of SPACFDPZ-DMAC in hexane, toluene, 1,4-dioxane, THF and neat film.

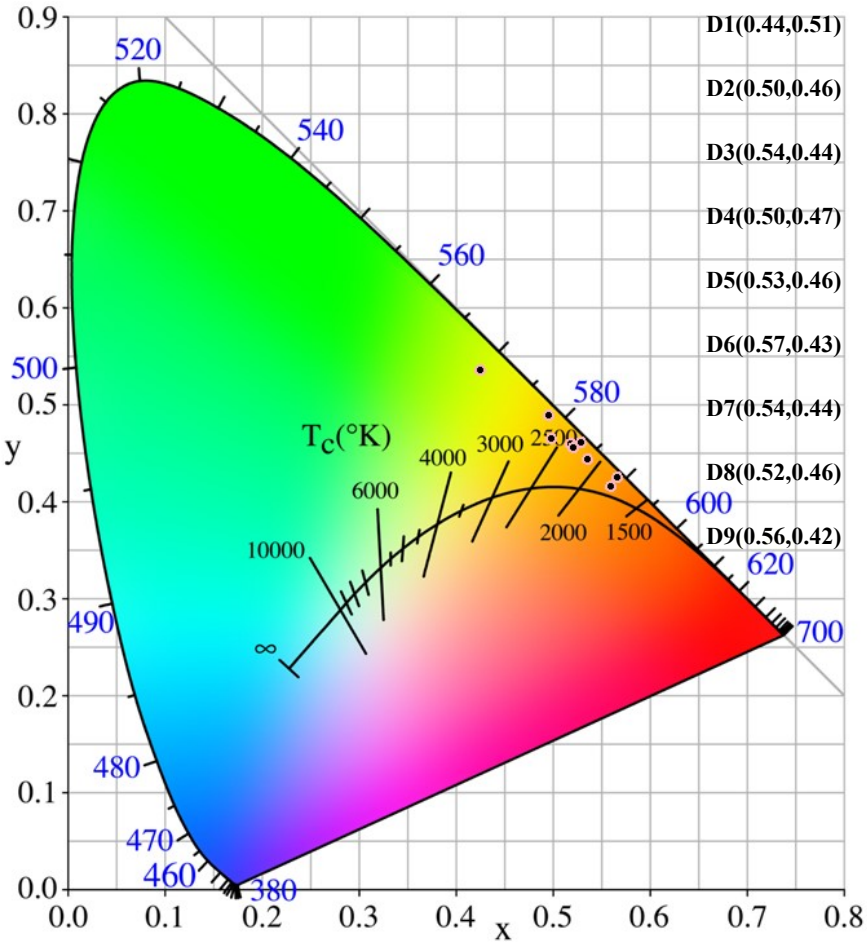

Figure S7. CIE coordinates of devices D1-D9.

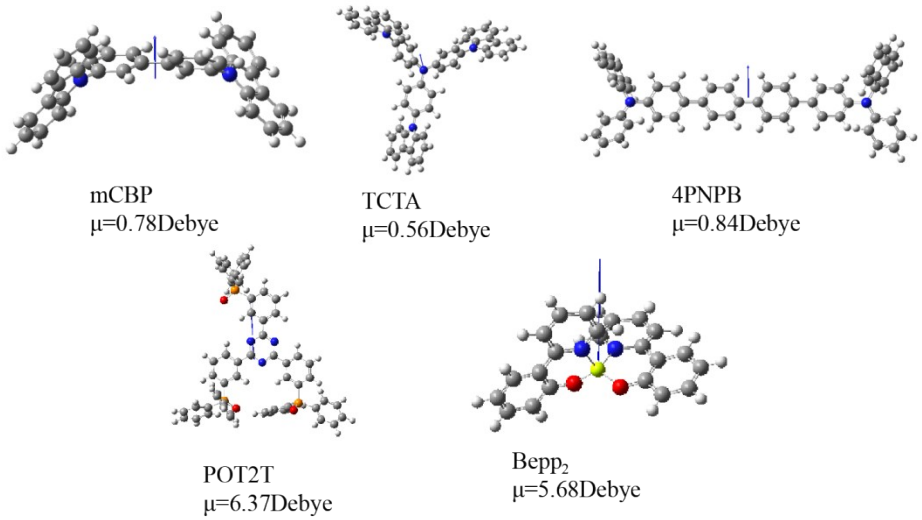

Figure S8. Dipole moment of hosts (calculated by optimizing the structure of the ground state molecules (method: B3LYP basic set: 6-31g d)).

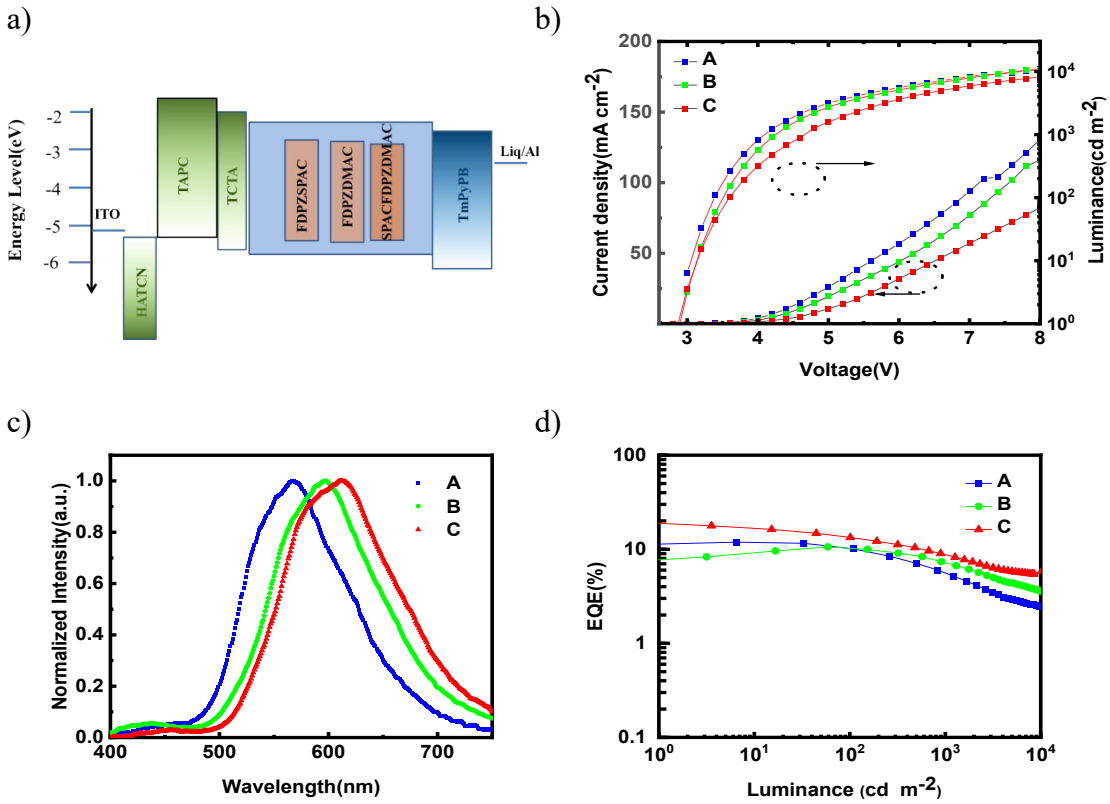

Figure S9. a) Device configuration and energy-level diagram of the resulting OLEDs based on $Bepp_2$ doped 5% FDPZ-SPAC(A), FDPZ-DMAC(B) and SPACFDPZ-DMAC(C). b) Current density −luminance−voltage (J−L−V) characteristics. c) EL spectra. d) EQE versus luminance characteristics.

devices	Current efficiency (Cd/A)	Power efficiency (lm/W)	EQE(%) [Max/1000 cd m^{-2}]	Max emission peak[nm]	CIE(x,y)[a]
$Bepp_2$:5% FDPZ2SPAC	41.2	43.1	11.9/5.2	567	(0.44,0.51)
$Bepp_2$:5% FDPZ2DMAC	28.3	26.1	10.6/6.5	597	(0.50,0.46)
$Bepp_2$:5% SPACFDPZ2DMAC	43.8	45.9	19.6/8.6	613	(0.54,0.44)

Table S3 EL performances of the resulting devices A-C.

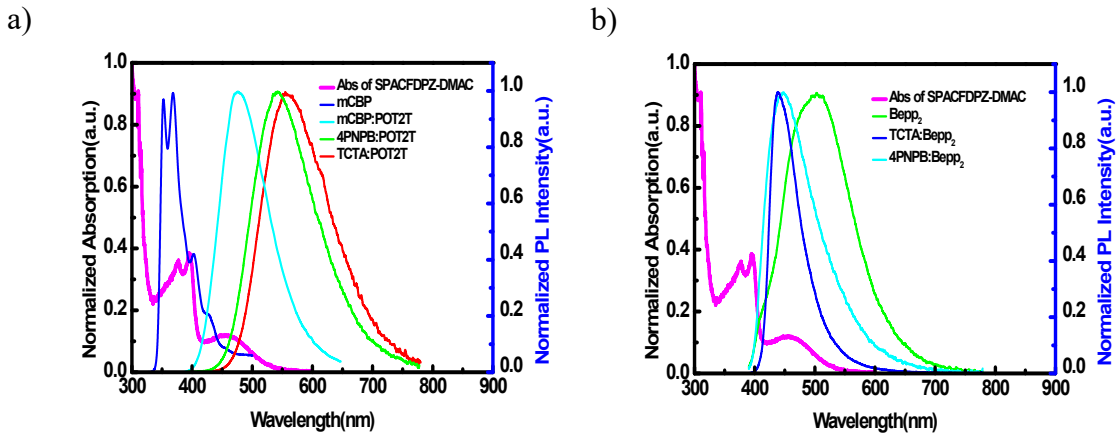

Figure S10. Normalized UV–vis absorption spectra of SPACFDPZ-DMAC and PL spectra of the used hosts.

	mCBP	mCBP:POT2T	4PNPB:POT2T	TCTA:POT2T	Bepp$_2$	4PNPB:Bepp$_2$	TCTA:Bepp$_2$
λ_{PL}(nm)	370	476	540	557	502	438	450

Table S4. PL peaks of the used hosts.

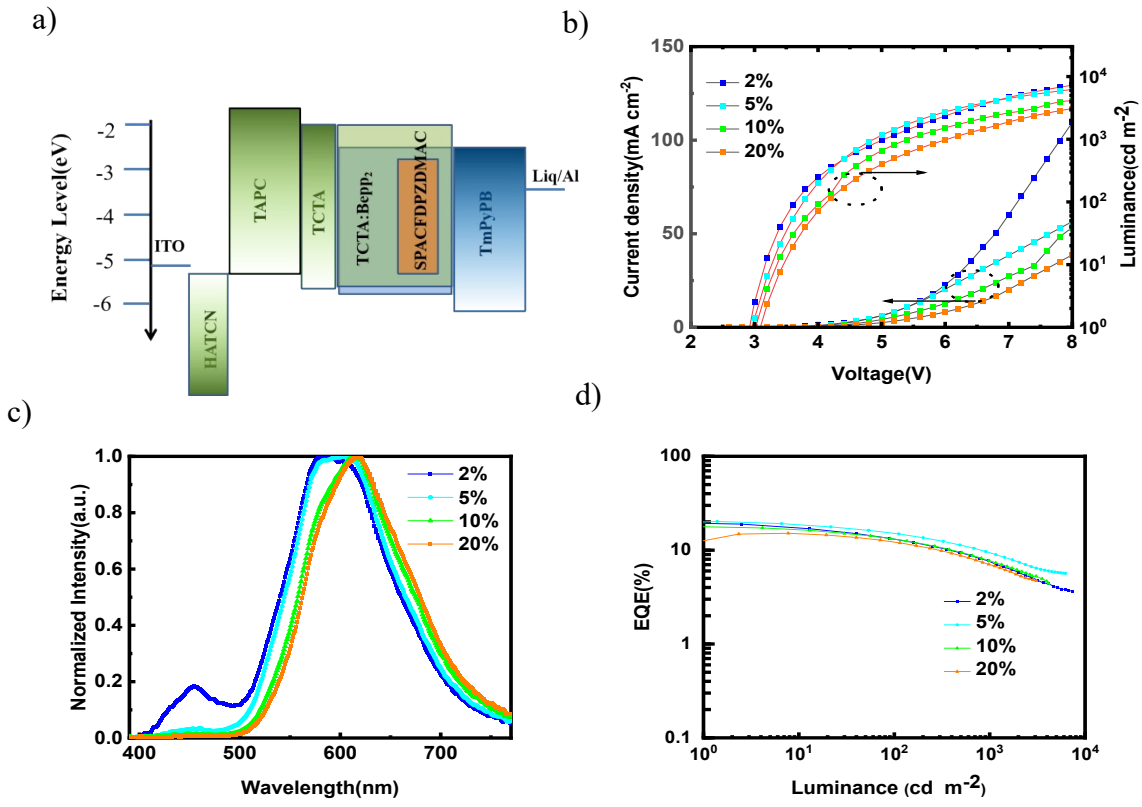

Figure S11. a) Device configuration and energy-level diagram of TCTA:$Bepp_2$: x% SPACFDPZ-DMAC OLEDs. b) Current density −luminance−voltage (J−L−V) characteristics. (c) EL spectra. d) EQE versus characteristics.

device	Current efficiency (Cd/A)	Power efficiency (lm/W)	EQE(%) [Max/1000 cd m^{-2}]	Max emission peak[nm]	CIE(x,y)[a]
TCTA:$Bepp_2$:2% SPACFDPZ2DMAC	48.1	53.9	19.8/7.5	581	(0.48,0.43)
TCTA:$Bepp_2$:5% SPACFDPZ2DMAC	46.2	51.8	20.2/9.3	602	(0.52,0.46)
TCTA:$Bepp_2$:10% SPACFDPZ2DMAC	33.3	34.8	17.8/7.7	614	(0.56,0.44)
TCTA:$Bepp_2$:20% SPACFDPZ2DMAC	26.4	25.9	15.1/6.8	616	(0.57,0.43)

Table S5 EL performances of the resulting OLEDs based on TCTA:$Bepp_2$ host doped SPACFDPZ2DMAC with different concentrations.

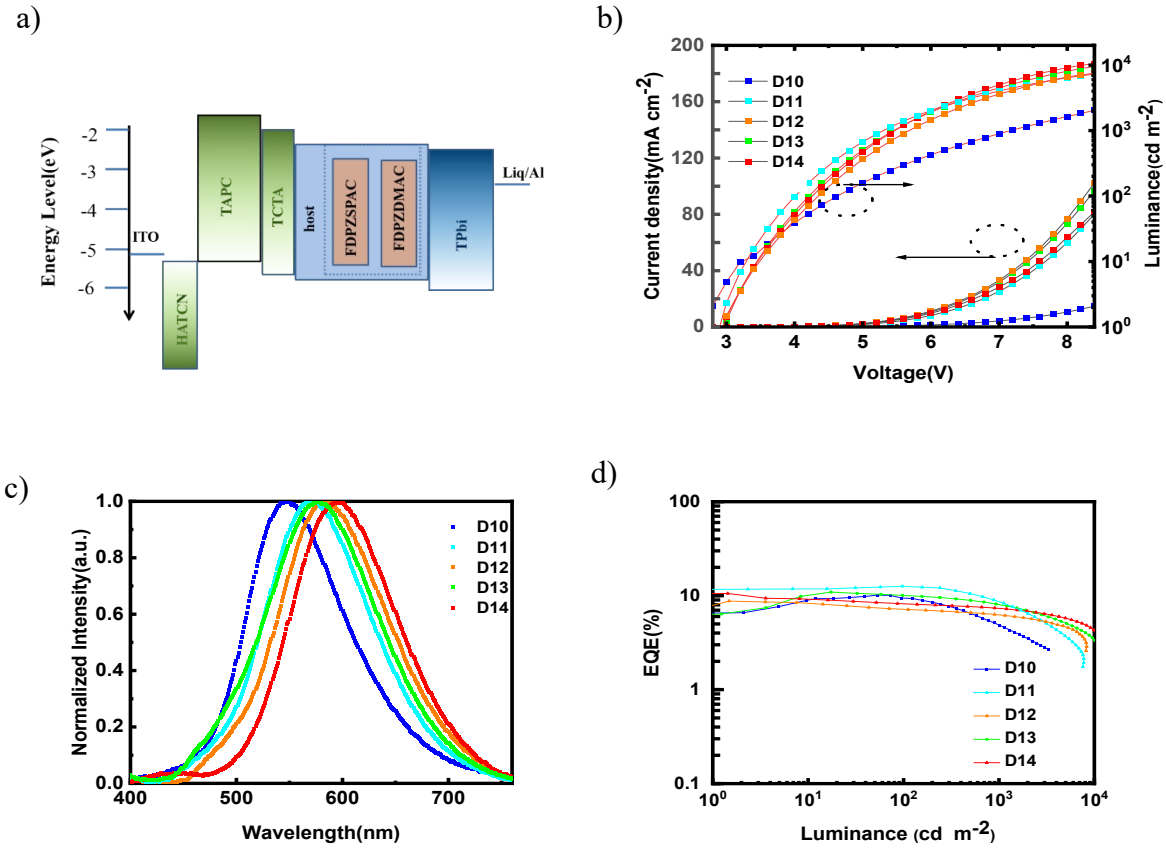

Figure S12. a) Device configuration and energy-level diagram of the resulting OLEDs. D10:TCTA:5% FDPZ-SPAC, D11:TCTA:Bepp$_2$:5% FDPZ-SPAC, D12: 4PNPB:Bepp$_2$:5% FDPZ-SPAC, D13:TCTA:Bepp$_2$:5% FDPZ-DMAC, D14:4PNPB:Bepp$_2$:5% FDPZ-DMAC. b) Current density −luminance−voltage (J−L−V) characteristics. c) EL spectra. d) EQE versus luminance characteristics.

devices	EML	Current efficiency (Cd/A)	Power efficiency (lm/W)	EQE(%) [Max/1000 cd m^{-2}]	Max emission peak[nm]	CIE(x,y)[a]
D10	TCTA: 5% FDPZ-SPAC	34.3	24.5	10.2/3.7	545	(0.39,0.53)
D11	TCTA:Bepp$_2$:5% FDPZ-SPAC	35.2	27.6	12.5/8.4	568	(0.44,0.50)
D12	4PNPB:Bepp$_2$:5% FDPZ-SPAC	21.9	22.9	8.8/6.3	579	(0.48,0.48)
D13	TCTA:Bepp$_2$:5% FDPZ-DMAC	36.4	31.8	10.9/7.9	577	(0.45,0.49)
D14	4PNPB:Bepp$_2$:5% FDPZ-DMAC	28.5	31.9	10.5/7.4	594	(0.51,0.46)

Table S6 EL performances of the resulting devices A-C.

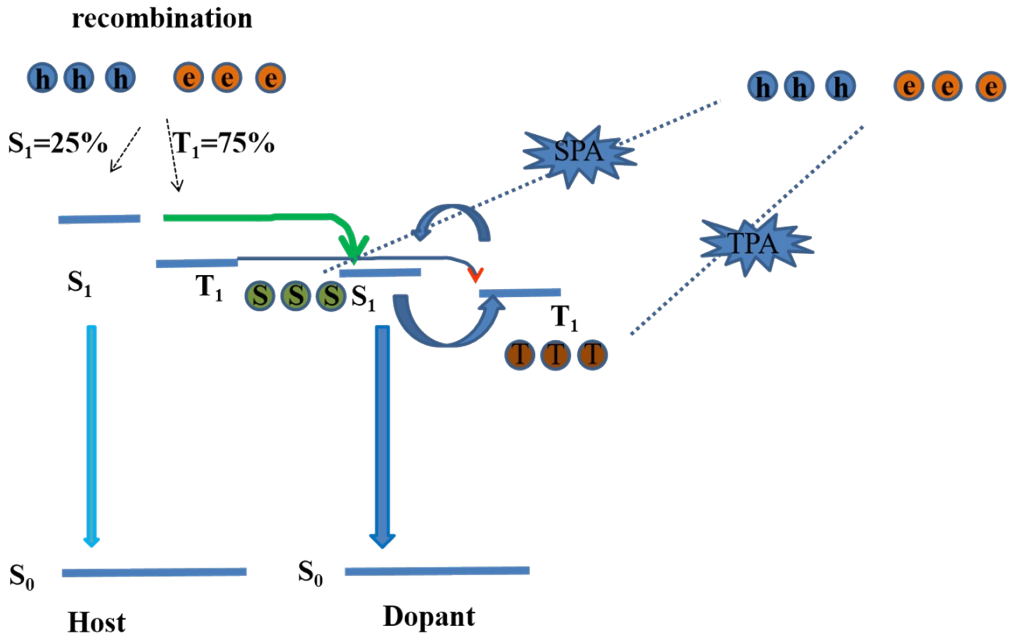

Figure S13. Main excited state annihilation pathways in the studied OLEDs.

Considering the main excited state annihilation pathways (SPA and TPA) associated with the TADF processes in OLEDs, the time evolution of singlet and triplet excited states can be modeled as

$$\frac{dP}{dt} = \frac{j}{ew} - k_L P^2 \quad (1)$$

$$\frac{dS}{dt} = Y(j)\frac{1}{4}k_L P^2 - \left(k_S + k_{ISC} + k_{NR} + k_{SP}P\right)S + k_{RISC}T \quad (2)$$

$$\frac{dT}{dt} = Y(j)\frac{3}{4}k_L P^2 - \left(k_{RISC} + k_{TP}P\right)T + k_{ISC}S \quad (3)$$

where k_L is the Langevin recombination rate expressed as

$$k_L = \frac{e(\mu_h + \mu_e)}{\varepsilon_0 \varepsilon_r} \quad (4)$$

e is the elementary charge, w is the width of the recombination zone, ε_0 and ε_r is the permittivity of free space and the relative permittivity, respectively, μ_h (μ_e) is the hole (electron) mobility of the emissive layer. k_{SP} and k_{TP} refer to the rate constants of SPA and TPA, respectively. Here we assume that the width of the recombination zone is 20 nm. To quantify the SPA and TPA annihilation rates, EQE can be expressed as

$$EQE = \frac{k_S S}{j/ew}\eta_{out} \quad (5)$$

η_{out} was calculated to be 0.25 for mCBP:5%SPACFDPZ-DMAC($\theta_{//}$=79%), and 0.28 for 4PNPB:Bepp$_2$:5%SPACFDPZ-DMAC($\theta_{//}$=85%). Y(j) is the charge balance factor as function of j. Y(j)=0.8 for device D3 and Y(j)=1 for device D9, k_{SP}=1.2*10^{-10}cm^{3}s^{-1}, k_{TP} 1.6*10^{-12}cm^{3}s^{-1}for device

D3,k_{SP}=8*10^{-11}cm^{3}s^{-1}, k_{TP} 1.6*10^{-12}cm^{3}s^{-1}for device D9(fitting with EQE).

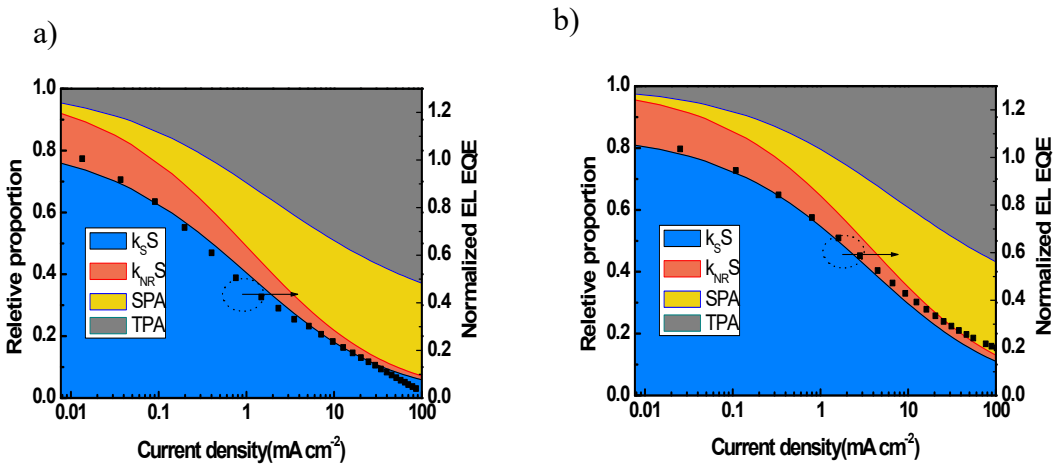

Figure S14. Relative contributions of the different excitonic processes and corresponding EQE in device a) D3 and b) D9.

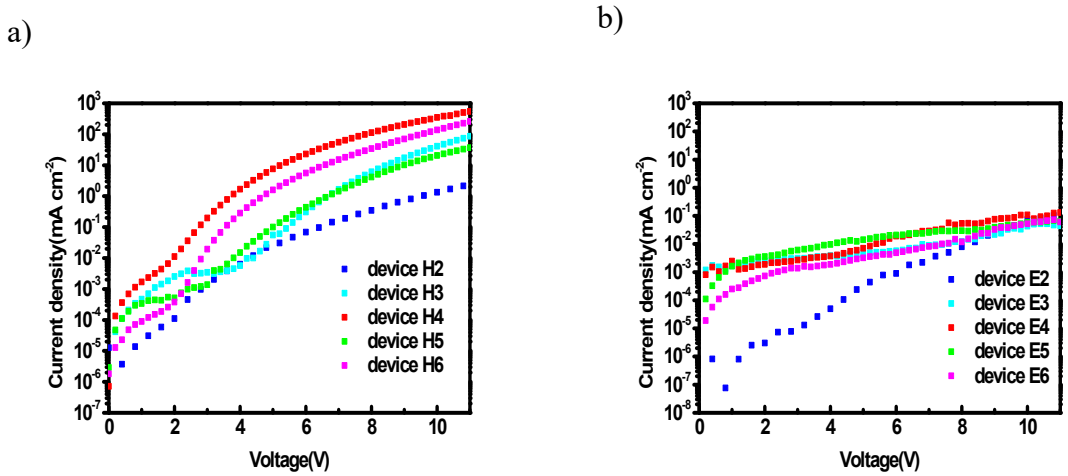

Figure S15. Current density–voltage curves of the hole-only and electron-only devices.

device H2：ITO/HAT-CN (5 nm)/ TAPC (10 nm)/ mCBP:2%SPACFDPZ-DMAC(50 nm)/ TAPC (10 nm)/ HAT-CN (5 nm)/ Al (100 nm)

device H3：ITO/HAT-CN (5 nm)/ TAPC (10 nm)/ mCBP:POT2T:2%SPACFDPZ-DMAC(50 nm)/ TAPC (10 nm)/ HAT-CN (5 nm)/ Al (100 nm)

device H4：ITO/HAT-CN (5 nm)/ TAPC (10 nm)/ Bepp$_2$:2%SPACFDPZ-DMAC (50 nm)/ TAPC (10 nm)/ HAT-CN (5 nm)/ Al (100 nm)

device H5：ITO/HAT-CN (5 nm)/ TAPC (10 nm)/ TCTA:Bepp$_2$:2%SPACFDPZ-DMAC (50 nm)/ TAPC (10 nm)/ HAT-CN (5 nm)/ Al (100 nm)

device H6：ITO/HAT-CN (5 nm)/ TAPC (10 nm)/ 4PNPB:Bepp$_2$:2%SPACFDPZ-DMAC (50 nm)/ TAPC (10 nm)/ HAT-CN (5 nm)/ Al (100 nm)

device E2：ITO/Liq (1 nm)/ TmPyPB(10 nm)/ mCBP:2%SPACFDPZ-DMAC (50 nm)/ TmPyPB (10 nm)/Liq (1 nm)/ Al (100 nm)

device E3：ITO/Liq (1 nm)/ TmPyPB(10 nm)/ mCBP:POT2T:2%SPACFDPZ-DMAC (50 nm)/ TmPyPB (10 nm)/Liq (1 nm)/ Al (100 nm)

device E4：ITO/Liq (1 nm)/ TmPyPB(10 nm)/ Bepp$_2$:2%SPACFDPZ-DMAC (50 nm)/ TmPyPB (10 nm)/Liq (1 nm)/ Al (100 nm)

device E5：ITO/Liq (1 nm)/ TmPyPB(10 nm)/ TCTA:Bepp$_2$:2%SPACFDPZ-DMAC (50 nm)/ TmPyPB (10 nm)/Liq (1 nm)/ Al (100 nm)

device E6：ITO/Liq (1 nm)/ TmPyPB(10 nm)/ 4PNPB:Bepp$_2$:2%SPACFDPZ-DMAC (50 nm)/ TmPyPB (10 nm)/Liq (1 nm)/ Al (100 nm)

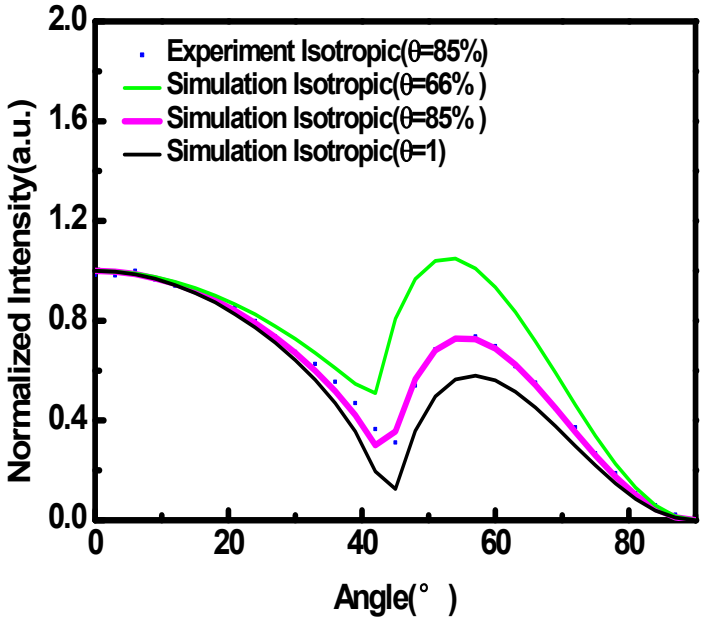

Figure. S16. Angle-dependent PL intensity of p-polarized light at peak emission from 30 nm thick 4PNPB:Bepp$_2$ doped **SPACFDPZ-DMAC** films.

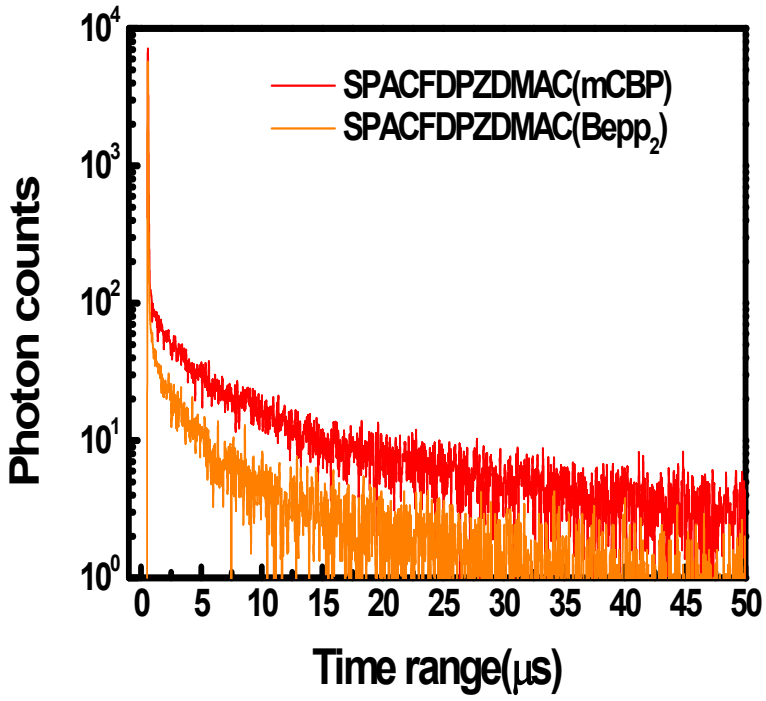

Figure S17. Transient PL decay curves of mCBP: 5% **SPACFDPZ-DMAC** and $Bepp_2$: 5% **SPACFDPZ-DMAC** films. Calculated k_{RISC}: $3.5*10^5$ s^{-1} for mCBP: 5% **SPACFDPZ-DMAC** and $5.3*10^5$ s^{-1} for $Bepp_2$: 5% **SPACFDPZ-DMAC**.

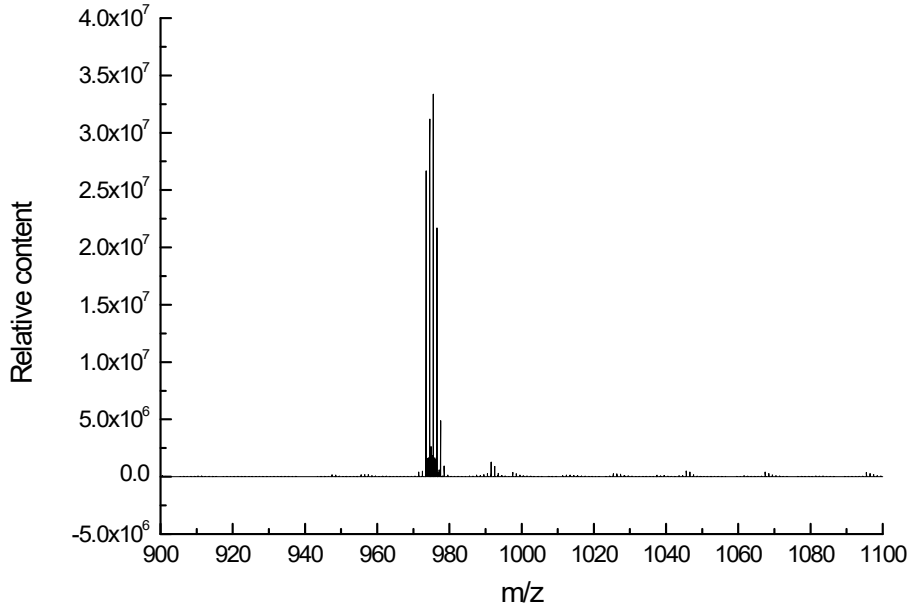

Figure S18. High-resolution mass spectrometry of **FDPZ-SPAC**.

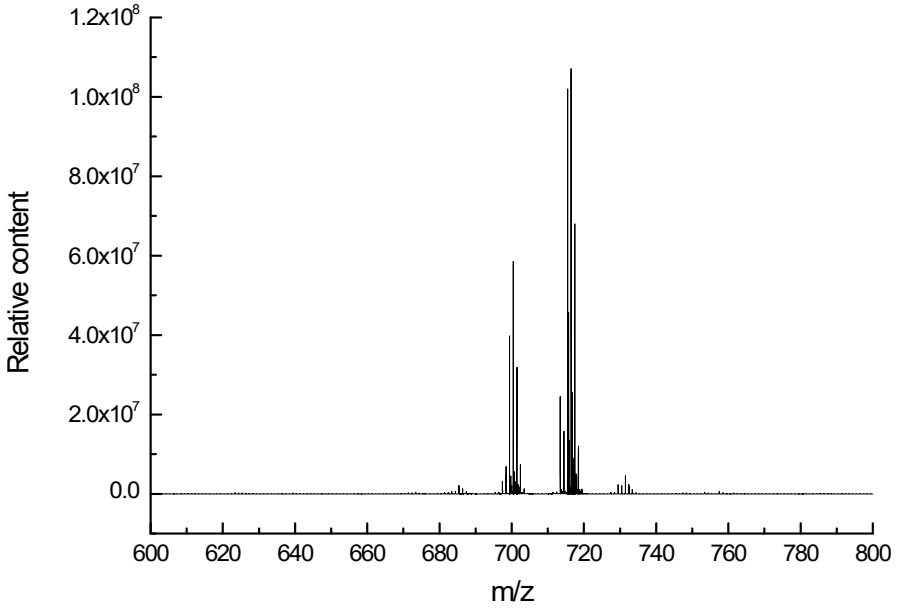

Figure S19. High-resolution mass spectrometry of **FDPZ-DMAC**.

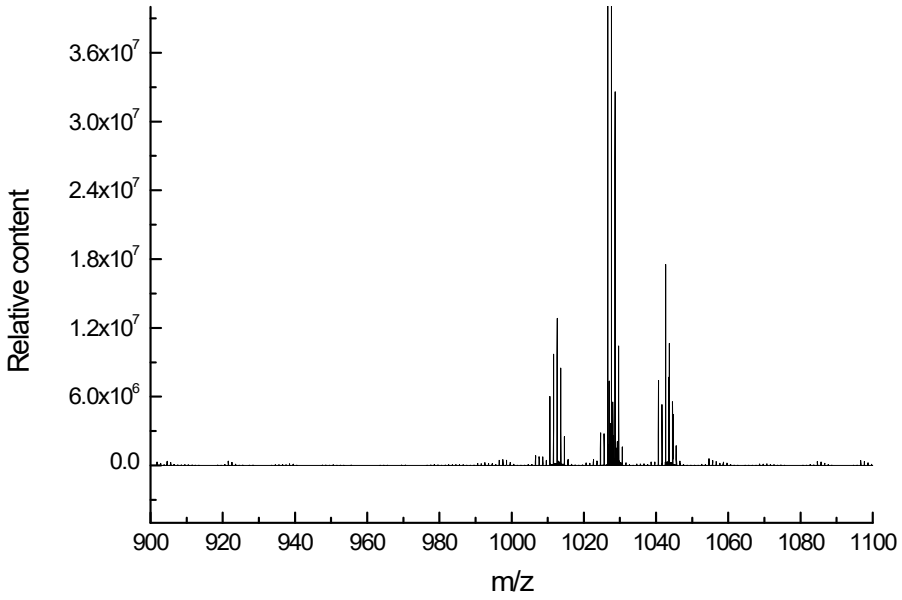

Figure S20. High-resolution mass spectrometry of **SPACFDPZ-DMAC**.

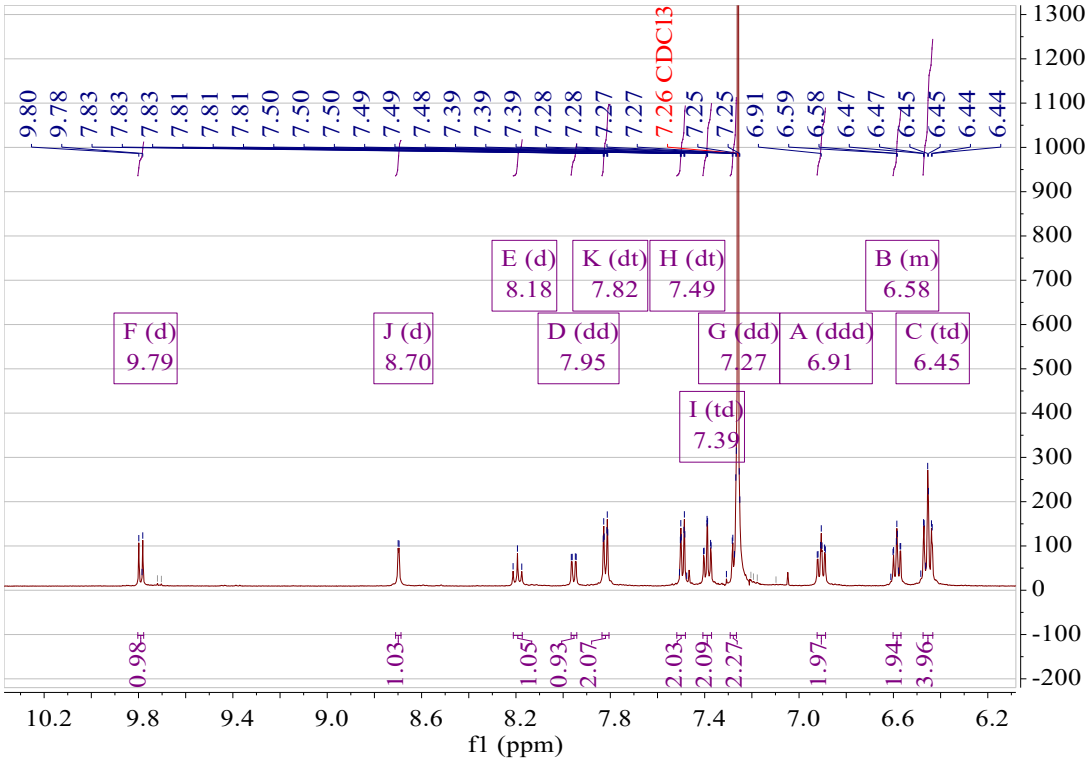

Figure S21. ^{1}H NMR spectrum of FDPZ-SPAC in $CDCl_3$.

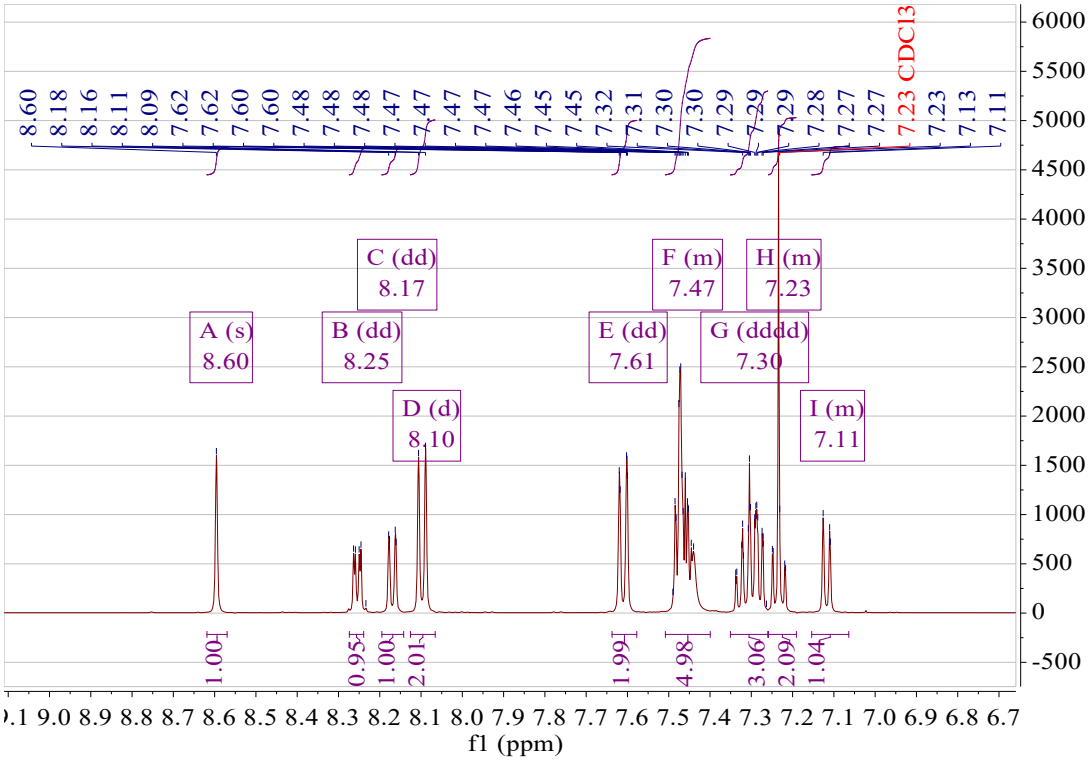

Figure S22. ^{1}H NMR spectrum of FDPZ-DMAC in $CDCl_3$.

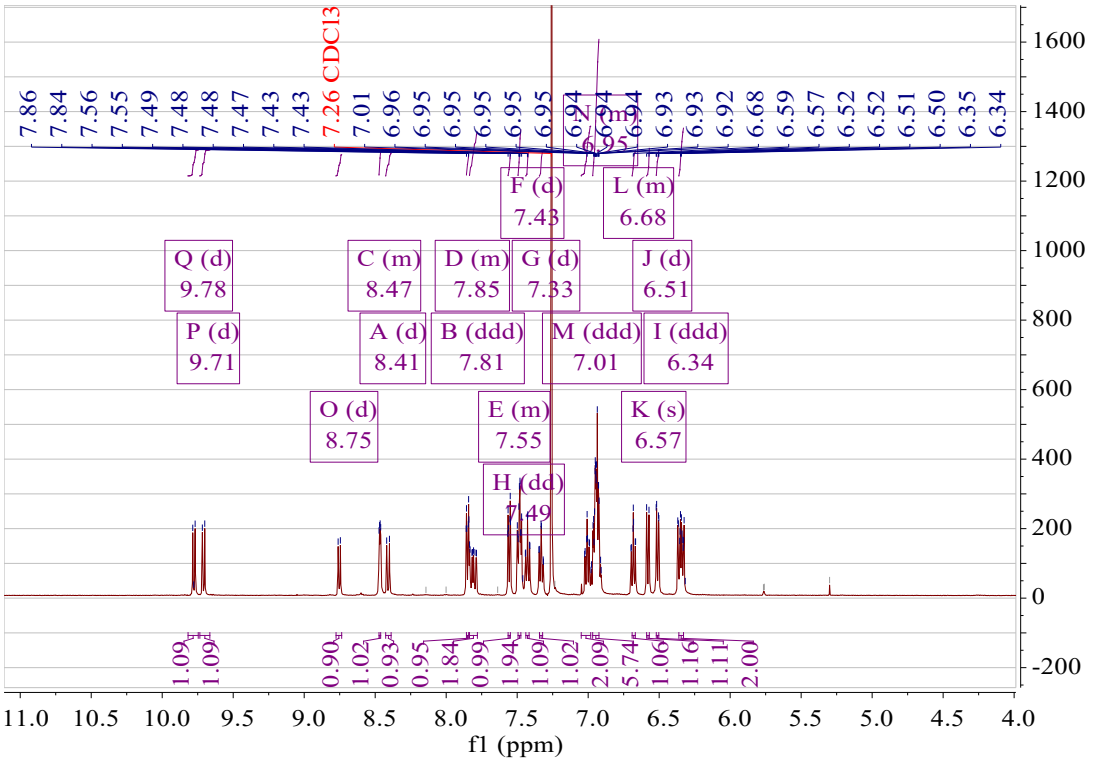

Figure S23. ^{1}H NMR spectrum of SPACFDPZ-DMAC in $CDCl_3$.

EML	λ_{em}	EQE_{max}	EQE_{1000}	Roll-off	References
CBP:10%DMAC-11-DPPZ	588	23.8%	~7%	71%	[38]
PBICT:5%FBPCNAc	614	17.4%	~9%	48%	[39]
mCPCN:15%PhNAI-PMSBA	610	22.3%	7.6%	66%	[40]
DBTTPI:1%5,8-DCNQx-DICz	603	12.5%	~8%	36%	[20]
CBP:8%oDTBPZ-DPXZ	604	20.1%	9.5%	52%	[41]
mCPCN:1.5%BFDMAc-NAI	590	20.3%	~5%	75%	[42]
CBP:12%dPhADBA	613	11.1%	~8%	28%	[33]
mCBP:5% SPACFDPZ2DMAC	581	15.5%	4.7%	70%	This Work

4PNPB:Bepp$_2$:5% SPACFDPZ2DMAC	614	21.1%	8.7%	58%	This Work

Table S7. EL $_{peak}$, EQE_{max}, EQE(1000 cd^{-2}) and Roll-off of the representative TADF red OLEDs with emission peaks between 580 and 650 nm.